Letters in Applied NanoBioScience
Open-Access Journal (ISSN: 2284-6808)

Article
Volume 12, Issue 2, 38
https://doi.org/10.33263/LIANBS122.038

Mill Scale as an Industrial Solid Waste for Preparing Iron Nano-Metal Powder as a Value-Added Product

Tarek A. Elbarbary [1,*]

[1] Central Metallurgical Research and Development Institute (CMRDI), P.O. Box 87 Helwan 11421, Cairo, Egypt
* Correspondence: tarekmmmm2012@yahoo.com (T.A.E.);

Scopus Author ID: 57344857300
Received: 28.11.2021; Accepted: 10.01.2022; Published: 16.03.2022

Abstract: A mill scale as a solid waste of the steel industry was used to obtain valuable products through hydrometallurgical processes. Mineral acids were employed for leaching the iron content. The affecting parameters of the leaching process such as solid/liquid ratio, temperature, time, and acid type and concentration were investigated. A 95% iron content was dissolved using 20% HCl at 60°C for 2 hrs. The process follows the liquid film kinetic model. Nano-iron powder was obtained by chemical reduction of the dissolved iron using sodium borohydride and polyacrylic acid at pH 9.5. The produced nano-iron can be employed as anti-bactericidal.

Keywords: mill scale; industrial waste; solid waste; iron powder; nano-iron particles.

1. Introduction

Solid wastes are generated widely. Many industrial sources of these wastes are residential, institutional, and industrial activities. Improper disposal of solid waste can create unsanitary conditions, which causes environmental pollution. It is essential to control waste from the metal and steel industry. There are many by-products of the steel companies. They are considered wastes that need extensive research to reuse [1]. A mill scale one of these by-products, which is produced due to the steel hot rolling process. It is a bluish-black solid composed of mixed iron oxides FeO, Fe_2O_3, and Fe_3O_4. It is flakes of less than 0.1 mm thickness [2]. The larger sizes were added to sintering plants, but it reduced the sinter productivity [3-5].

It is considered an oxidizer in the conventional electric arc furnaces through the steel-making process. Recently, the electric arc furnaces were modified with enhancing melting systems and oxidation processes which are more efficient than mill scale [6-10]. Although mill scale was employed as an additive in cement plants, it does not uniformly mix with the other materials due to its higher density. Thus, it causes a greater variation in the blend of the kiln feed [11].

The mill scale was used to prepare iron metal powder of 98% purity by reducing carbon monoxide gas (CO) at 1050°C for 3 hrs. Hydrogen reduction reduced carbon and oxygen contents to acceptable values (0.23% and 0.28%) [8]. Recently, the mill scale was converted to sponge iron through reduction by coke at different temperatures and times. Sponge iron was successfully applied in electric furnaces, but there is no technology for that [9-10].

The agglomeration and unstable of nanoparticles are expected due to their superior small size. So, the nanoparticle preparation and application processes are restricted and limited. To avoid that, a surface modification must be carried out using a suitable surface modifier with chemically function groups such as amine or carboxylic groups. The iron nanoparticles are chemically active to react with a different functional group such as stabilizer, surfactant, and steric polymers. Thus, they have a higher potential for surface modification [12].

This work aimed to recover iron from the mill scale through leaching in hydrochloric acid to produce ferric chloride. It's application as an adsorber for wastewater treatment was investigated. Also, nano-iron particles' preparation by reducing ferric ions for microbial application was investigated.

2. Materials and Methods

2.1. Materials.

Iron & Steel Co., Egypt supplied a 20 kg of representative mill scales sample was supplied by Iron & Steel Co., Egypt. from the hot rolling section. Hydrochloric acid of 32% purity was supplied by Fisher Scientific. Using a ball mill, the whole mill scale sample was ground to less than 75 microns. Iron metal powder of 98% purity and particle size less than 45 microns was supplied by Promotion powders, India. All other chemicals such as sodium boro-hydride and absolute ethyl alcohol were supplied by Sigma Aldrich. Microbial strains included *Staphylococcus aureus, Escherichia coli, Pseudomonas aeruginosa, Proteus mirabilis, Enterococcus faecalis, Klebsiella pneumoniae, Bacillus subtilis, Bacillus cereus, Salmonella typhimurium,* and *Shigellaflexneri* were supplied by Sigma Aldrich.

2.2. Methods.

2.2.1. Leaching and nano-iron preparation.

The acid leaching process was carried out in a 250 cm^3 glass reactor fitted with a mechanical stirrer (K –EUROSTAR DIGITAL IKA-WERKE). Hydrochloric or sulfuric acids of required concentration were placed in the reactor, and then the desired weight of the mill scale was added. The mixing was carried out at the desired temperature for the desired time at 200 rpm. After mixing, the mixture was filtered, followed by washing with distilled water.

The preparation of nano-iron particles was carried out using sodium borohydride as a reducing agent in the presence of polyacrylic acid as a dispersing agent to avoid the aggregation of nanoparticles.

2.2.2. Characterization.

X-Ray Diffractometer (Germany) Model AXS D8 with Cu-target (λ=1.540 Å and n=1) at 40 kV potential and 40 A was employed to characterize the mineral structure of the sample. The diffraction data were recorded for 2θ values between 10° and 80°, and the scanning rate was 3° min^{-1} or 0.02°/0.4 sec.

The determination of iron content was carried out by the complex method with EDTA using salicylic acid as an indicator [11]. The atomic absorption AAnalyst-200 was employed to analyze the digested sample in a 20% hydrofluoric acid solution.

Investigation of the surface morphology of the prepared nano-iron particles was investigated by JEOL instrument (Japan) model JSM-5410 scanning electron microscope (SEM) at 15 kV of excitation potential.

2.2.3. Microorganisms test.

The microbial test was carried out according to Agar Diffusion Method (ADM). A 20 ml of nutrient agar medium were seeded in 100 µl of *Staphylococcus aureus* (ATCC-29213), *Escherichia coli* (ATCC-25922), *Pseudomonas aeruginosa* (ATCC-27953), *Proteus mirabilis* (ATCC 9240), Enterococcus *faecalis* (ATCC 29212), *Klebsiella pneumoniae* (ATCC-13883), *Bacillus subtilis* (ATCC 6633), *Bacillus cereus* (ATCC 6629), *Shigella flexneri* (ATCC 12022), *Salmonella typhimurium* (ATCC 14028) strains.

The wells were cut using a sterile cork borer of 9 mm diameter and 100 µl of 1% nano-iron solution to assay the antimicrobial activity against each test strain. The results were recorded after incubation at 37°C for one day [13].

3. Results and Discussion

3.1. Characterization of waste PCBs.

Figure 1 and Table 1 show the composition of the mill scale sample using the XRD and XRF analyses. The results showed that iron represents the main component of the sample (96.5%) as iron oxide. Also, traces of Si, Al, K, Mn, Ti, Mg, Na, P, Ca, Cu, and sulfur were detected. The size analysis of the ground sample showed that 50% of the sample has a particle size less than 1 mm while about 70% is less than 2 mm, Figure 2.

Table 1. Chemical composition, wt% of the mill scale sample.

Item	**Fe**	**Fe_2O_3**	**SiO_2**	**Al_2O_3**	**K_2O**	**MnO**	**Cr_2O_3**	**S**
%	67.55	96.5	0.68	0.16	0.012	l.022	0.14	0.013
Item	**TiO_2**	**MgO**	**Na_2O**	**P_2O_5**	**CaO**	**CuO**	**LOI**	
%	0.013	0.10	0.04	0.074	0.13	0.4	1.1	

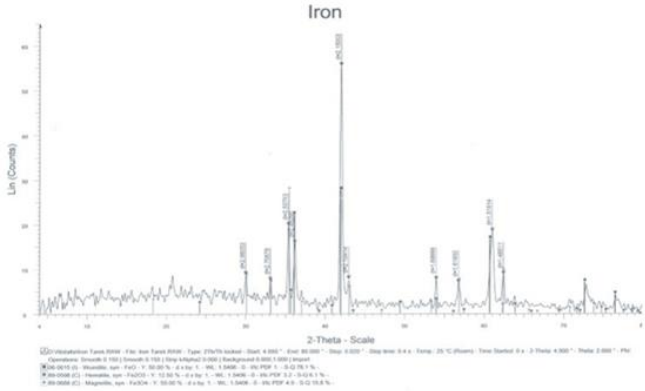

Figure 1. XRD analysis of mill scale sample.

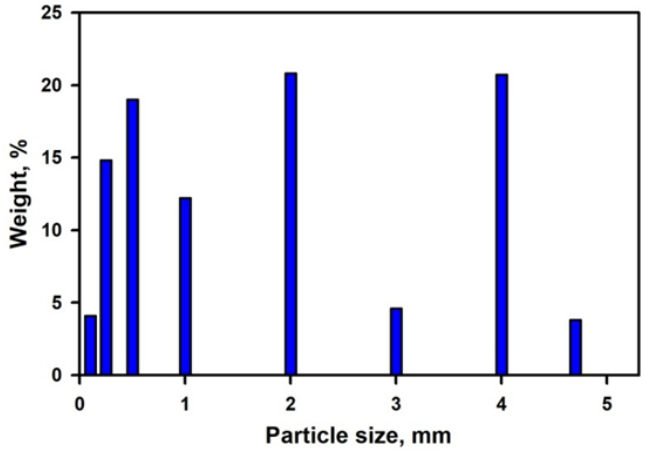

Figure 2. Sieve analysis of the crushed mill scale sample.

3.2. Leaching of mill scale.

The most affecting parameters of the leaching process, such as acid type and concentration and quantity of mill scale, time, and temperature, were studied. The gas evolution through the dissolution of the mill-scale sample is highly reductive. Thus, the hydrochloric acid leaching process includes a pre-leach thermal treatment and acid leaching that extracts the iron from the mill scale to form soluble ferrous chloride [14].

3.2.1. Effect of acid type and concentration.

Figure 3 shows the effect of acid type and concentration on iron dissolution. The extraction was increased by increasing the acid concentration. An 85% of the iron was extracted in 20% hydrochloric acid at 30°C for 60 min. The dissolution is reduced in more concentrated HCl acid [15]. On the other hand, the extraction efficiency in 30% sulfuric acid was 70%. The higher dissolution in HCl acid may be due to the oxidation power of chloride ions. The amount of acid and its concentration are important for economic issues [16].

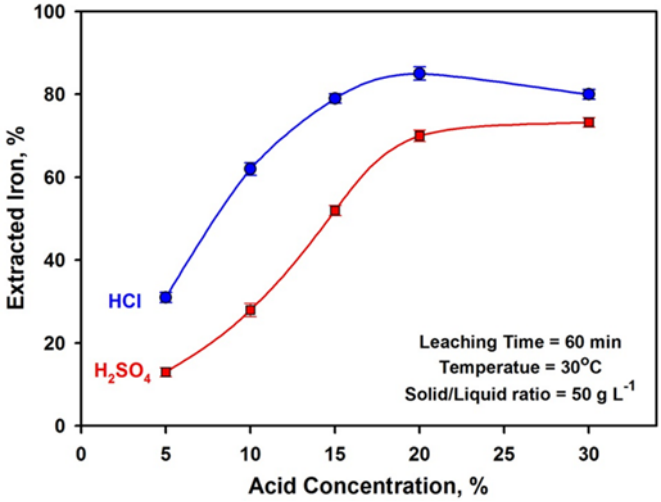

Figure 3. Effect of acid type and concentration on iron dissolution.

3.2.2. Effect of solid/liquid ratio.

Figure 4 shows the effect of solid/liquid ratio (quantity of mill scale) on the iron dissolution at a different hydrochloric acid concentration at 60 min and 30°C. As expected before, the iron dissolution increases with increasing the acid concentration. In contrast, the dissolution was decreased with increasing the quantity of mill scale. This may be due to insufficient acid species attacking iron atoms at this lower acid concentration [8].

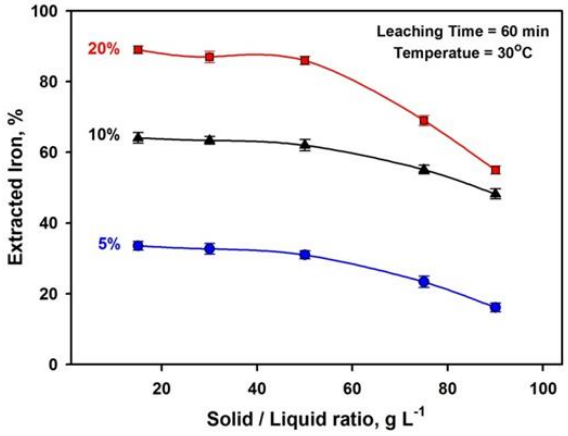

Figure 4. Effect of solid/liquid ratio on iron dissolution as a function of HCl concentration.

3.2.3. Effect of leaching time and temperature.

Figure 5 shows the effect of contact time on iron dissolution as a function of temperature. The iron dissolution is increased rapidly with increasing temperature. It may be due to the reactions in leaching being exothermic [17]. The hydrochloric acid leaching process consists of a pre-leach thermal treatment. The dissolution of iron was occurred in two stages: an initially rapid dissolution of the iron and a slower dissolution. This initially rapid rate of iron extraction is altered by process liquor conditions [8]. The maximum dissolution of iron of about 95% was achieved after 2 hrs in 20% HCl at 60°C. The increasing rate is due to the continuous oxidation of metal atoms to metal ions until saturation. The metal atoms in the solid mill-scale act as a reductant and are able to reduce hydrogen gas in the acidic solution, which has been observed as vigorous gas generation during leaching [18].

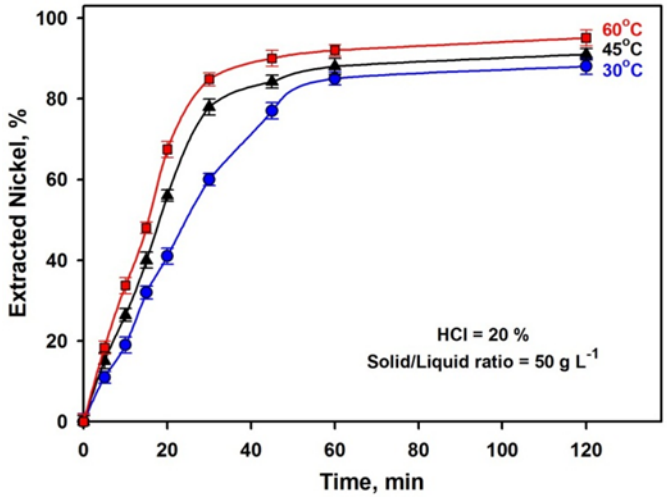

Figure 5. Effect of leaching time on iron dissolution as a function of temperature.

3.2.4. Kinetic study.

The leaching of iron in acid is expressed as:

$$aA\ \text{liquid} + bB\ \text{solid} = \text{Product}$$

where a, b, A and B represent the stoichiometric coefficients. The shrinking core model describes the kinetics of leaching reaction, wherein a reaction between solid and fluid on the solid surface. A fluid film surrounds the solid particles so a mass transfer occurs between the solid and the bulk fluid. As the reaction proceeds, the unreacted core of the solid shrinks towards the solid center, and a porous product layer forms around the unreacted core. If the reaction is controlled by diffusion through a liquid film, the integrated rate equation is [19]:

$$X = K_l \cdot t$$

If the reaction is controlled by a surface chemical reaction, the integrated rate equation is [20]:

$$1- [(1-X)]^{1/3} = K_r \cdot t$$

If the reaction is controlled by diffusion through a product layer, the integrated rate equation is [21]:

$$1\text{-}3\ (1-X)^{2/3} + 2(1-X) = K_d \cdot t$$

If the reaction is controlled by a mixed kinetic model, the integrated rate equation is [21]:

$$([1-(1-X)\text{^}(1/3)])^2 = K_m \cdot t$$

where X is the conversion fraction of solid particles, K_l is the apparent rate constant for the liquid film, K_r is the apparent rate constant for the surface chemical reaction, K_d is the apparent rate constant for the diffusion through a product layer, K_m is the apparent rate constant for the mixed kinetic model and t is the reaction time.

To determine the kinetic parameters and rate controlling step of iron leaching, the experimental data were analyzed using the above models. Table 2 summarizes the results of fitting kinetic models (Figures 6-9). It showed that the liquid film is a more suitable model for demonstrating the kinetics of the iron leaching system.

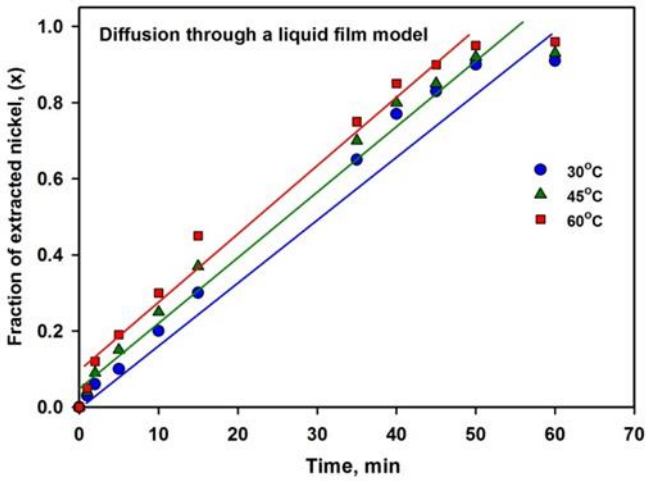

Figure 6. Fitting results by the diffusion through a liquid film model.

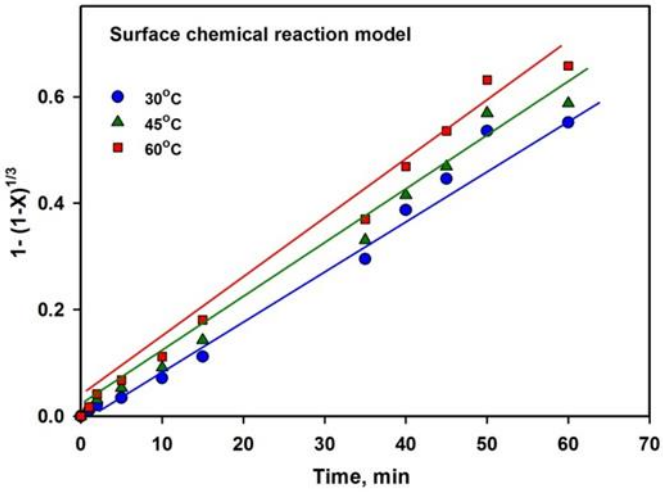

Figure 7. Fitting results by the surface chemical reaction model.

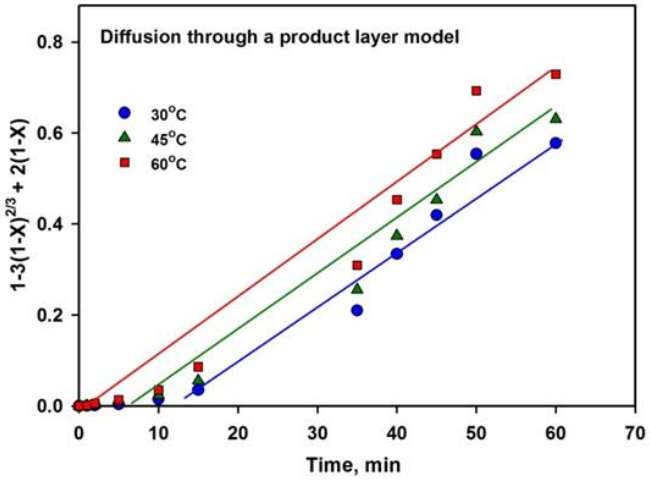

Figure 8. Fitting results by the diffusion through a product layer model.

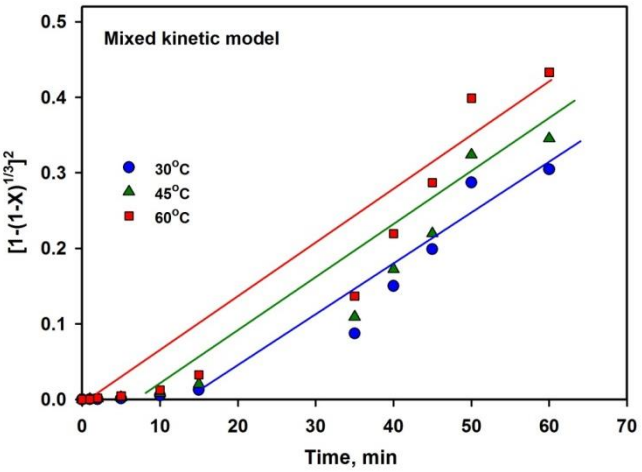

Figure 9. Fitting results by the diffusion through a liquid film model.

Table 2. The kinetic parameters and rate-controlling step of iron leaching.

Model	Parameter	30°C	45°C	60°C
Diffusion through a liquid film	R^2	0.9932	0.9916	0.9908
	K_1	0.0157	0.0162	0.0165
Surface chemical reaction	R^2	0.9251	0.9223	0.9213
	K_r	0.0083	0.0099	0.0103
Diffusion through a product layer	R^2	0.8946	0.8893	0.8742
	K_d	0.0077	0.0102	0.0111
Mixed kinetic model	R^2	0.8126	0.8107	0.8081
	K_m	0.0036	0.0052	0.0058

3.3.Morpholgy of prepared iron nonoparticles.

The pH of the solution is a significant effect on the particle diameter. The resulting iron nanoparticles were in nano-scale (less than 100 nm) at a pH of 9.5 [12]. Figure 10 shows the iron nanoparticles images through a scanning electron microscope. It shows the particle size distribution, and the particle size could be measured precisely. Single particles with no agglomeration effect existed. The particle size distribution was in the range of 35–72 nm, with more particle sizes in the range of 38–139 nm. It was also confirmed that impurities had not been introduced into the sample during the formation process. It could be clearly seen that the particles were slightly agglomerated together. The size of the agglomeration particles obtained from SEM micrograph was inconsistent. Also, the iron nanoparticles were analyzed by the transmission microscope, Figure 11. The red areas indicate the iron, while the other may be due to iron oxide and magnetite.

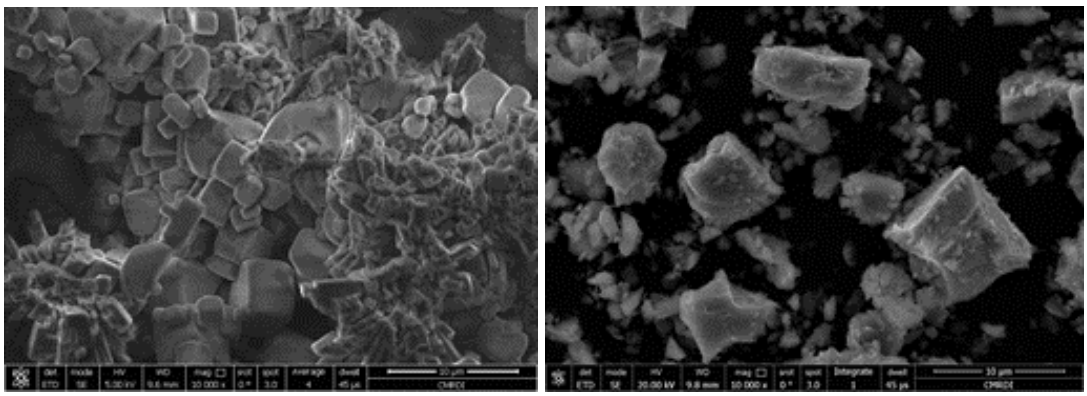

Figure 10. SEM images of the prepared iron nanoparticles.

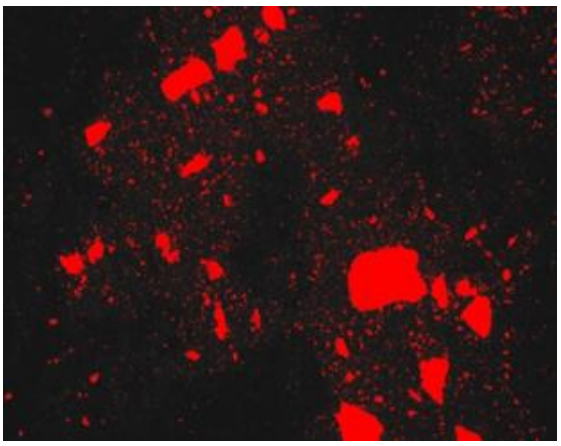

Figure 11. Transmission microscope image of the prepared iron nanoparticles.

3.4. Microbial effect of iron nanoparticles.

The performance of iron nanoparticles as bactericidal was studied and compared with other metals such as silver. The results are tabulated in Table 3. The results showed that the prepared iron nanoparticles have a higher bactericidal effect compared to other types of metals.

Table 3. The antimicrobial of prepared iron nanoparticles with other metals.

Type of microorganism	Nano-iron	Nanosilver	Chitin
S. aureus	-	17	23
E.coli	17	22	22
E.faecalis	16	20	22
P. mirabilis	-	-	-
p. aeruginosae	-	20	27
k. pneumonia	18	26	-
B.cereus	-	17	24
B.subtilis	17	20	22
S.flexneri	-	26	24
S. typhimurium	-	19	24

4. Conclusions

The mill scale is mainly composed of iron (96.5%) as iron oxide with Si, Al, K, Mn, Ti, Mg, Na, P, Ca, Cu and sulfur. The mill scale could be converted to ferric chloride through 20% HCl acid leaching at 60°C.

An 85% of iron could be extracted in 20% hydrochloric acid at 30°C for 1 hr while the extraction efficiency was 70% in 30% sulfuric acid. The dissolution of mill scale is a highly reductive process due to gas evolution. The hydrochloric acid leach process consists of a pre-leach thermal treatment. The dissolution occurred in two stages: an initially rapid dissolution of iron and a slower dissolution. This initially rapid rate of iron extraction is altered by process liquor conditions. The maximum dissolution (95%) was achieved after 120 min in 20% HCl at 60°C.

The kinetic study showed that the liquid film is a more suitable model for demonstrating the kinetics of the iron leaching system. The iron nanoparticles were prepared through a chemical reduction method of ferric chloride solution. The sodium borohydride was used as a reducing agent in the presence of polyacrylic acid as the dispersing agent at pH 9.5. The iron nanoparticles were in nano-scale (less than 100 nm) at a pH of 9.5. The prepared iron nanoparticles have a higher bactericidal effect than other metals.

Funding

This research received no external funding.

Conflicts of Interest

The authors declare no conflict of interest.

References

1. Agyeiwaah, E. The contribution of small accommodation enterprises to sustainable solid waste management, *J. Hospitality & Tourism Manag.* **2020**, *44*, 1-9, https://doi.org/10.1016/j.jhtm.2020.04.013.
2. Viet, N.H.; Quynh, P.N.D.; Oanh, N.T.H. Reduction Kinetics of Mill Scale Briquettes by Using A3 Fine Coal as a Reductant. *J Nanosci Nanotechnol* **2021**, *21*, 2563-2567, https://doi.org/10.1166/jnn.2021.19101.
3. Khanna, R.; Konyukhov, Y.V.; Ikram-Ul-Haq, M.; Burmistrov, I.; Cayumil, R.; Belov, V.A.; Rogachev, S.O.; Leybo, D.V.; Mukherjee, P.S. An innovative route for valorising iron and aluminium oxide rich industrial wastes: Recovery of multiple metals. *J. Environ Manage* **2021**, *295*, 113035, https://doi.org/ 10.1016/ j.jenvman.2021.113035.
4. Eissa, M.; Ahmed, A.; El-Fawkhry, M. Conversion of Mill Scale Waste into Valuable Products via Carbothermic Reduction. *Journal of Metallurgy* **2015**, *2015*, 926028, https://doi.org/10.1155/2015/926028.
5. Farahat, R.; Eissa, M.; Megahed, G.; Baraka, A. Reduction of mill scale generated by steel processing. *Steel Grips* **2010**, *8*, 88-92. https://www.researchgate.net/publication/288874180
6. Young, R.D.;Norris, D. Process for using mill scale in cement clinker production. US6709510B1**2004**.
7. Benchiheub, O.; Said, M.; Serrai, S.; Khalifa, M. Elaboration of iron powder from mill scale. *J. Materials & Environmental Science* **2010**, *1*, 267-276. https://www.researchgate.net/publication/267721953.
8. Martín, M.I.; Lpez, F.; Torralba, J. Production of sponge iron powder by reduction of rolling mill scale. *Ironmaking & Steelmaking* **2012**, *39*, 155-162, https://doi.org/10.1179/1743281211Y.0000000078.
9. Septiani, A.I.;Idayanti, N.; Kristiantoro, T.; Mada, D.; Kartika, N.L.; Mulyadi, D.; Rusmana, A.; Sumpena, P. Structural, Magnetic, and X-Band Microwave Absorbing Properties of Ni-Ferrites Prepared Using Oxidized Mill Scales. *J. Elektronika dan Telekomunikasi* **2021**, *21*, 27-34, https://doi.org/10.14203/ jet. v21.27-34.
10. Drummer, S.; Madzimbamuto, T.; Chowdhury, M. Green Synthesis of Transition-Metal Nanoparticles and Their Oxides: A Review. *Materials (Basel)* **2021**, *14*, 2700, https://doi.org/10.3390/ma14112700.
11. Sen, R.; Pandel, U. Closed crucible reduction of lump powdered mill scale or iron ore by coal: The sequential methodology and mechanism for optimization of process parameters. *Advanced Powder Technology* **2020**, *31*, 3760-3773, https://doi.org/10.1016/j.apt.2020.07.017.
12. Ismail, I.; Abdullah, A.H.; Abdul Arifin, A.S.; Ibrahim, I.R.; Shafiee, F.N.; Azis, R.a.S. Phase, morphological, and magnetic properties of iron oxide nanoparticles extracted from mill scale waste and its surface modification with CTAB surfactant. *Journal of the Australian Ceramic Society* **2020**, *56*, 729-743, https://doi.org/10.1007/s41779-019-00391-x.
13. Ali, E.; Almagboul, A.; Khogali, S.; Gergeir, U. Antimicrobial Activity of Cannabis sativa L. *Chinese Medicine* **2012**, *03*, 61-64, https://doi.org/10.4236/cm.2012.31010.
14. Yang, H.; Yoon, S.; Kim, Y.; Park, H.; Huh, S.; Hur, N. Recovery of iron oxide and calcium chloride from an iron-rich chloride waste using calcium carbonate. *Journal of Material Cycles and Waste Management* **2020**, *23*, 222-230, https://doi.org/10.1007/s10163-020-01119-x.
15. Korkmaz, K.; Alemrajabi, M.; Rasmuson, Å.; Forsberg, K. Recoveries of Valuable Metals from Spent Nickel Metal Hydride Vehicle Batteries via Sulfation, Selective Roasting, and Water Leaching. *Journal of Sustainable Metallurgy* **2018**, *4*, 313-325, https://doi.org/10.1007/s40831-018-0169-1.
16. Tzanetakis, N.; Scott, K. Recycling of nickel–metal hydride batteries. I: Dissolution and solvent extraction of metals. *J. Chemical Technology and Biotechnology* **2004**, *79*, 919-926, https://doi.org/10.1002/jctb.1081.
17. Porvali, A.; Ojanen, S.; Wilson, B.; Serna, R.; Lundström, M. Nickel Metal Hydride Battery Waste: Mechano-hydrometallurgical Experimental Study on Recycling Aspects. *Journal of Sustainable Metallurgy* **2020**, *6*, 78-90, https://doi.org/10.1007/s40831-019-00258-2.
18. Tao, L.; Wang, L.; Yang, K.; Wang, X.; Chen, L.; Ning, P. Leaching of iron from copper tailings by sulfuric acid: behavior, kinetics and mechanism. *RSC Advances* **2021**, *11*, 5741-5752, https://doi.org/10. 1039/D0RA08865J.
19. Arslan, V. A study on the dissolution kinetics of iron oxide leaching from clays by oxalic acid. *Physico-chemical Problems of Mineral Processing* **2021**, *57*, 97-111, https://doi.org/10.37190/ppmp/135749.
20. Shi, Z.Z.; Wang, M.R.; Zhang, G.K.; Zhang, L. Leaching and Kinetic Modeling of Pyrite Cinder in Sulphuric Acid. *Asian J. Chemistry* **2013**, *25*, 105-109, https://doi.org/10.14233/ajchem.2013.12810.
21. Wang, J.; Faraji, F.; Ghahreman, A. Effect of Ultrasound on the Oxidative Copper Leaching from Chalcopyrite in Acidic Ferric Sulfate Media. *Minerals* **2020**, *10*, 633, https://doi.org/10.3390/min10070633.